Quantum Yield Enhancement in Photocatalytic HCOOH Decomposition to H_2 under Periodic Illumination

Sie Shing Wong[a,b], Max Joshua Hülsey[b], Hua An[a,b], Ning Yan[b,*]

[a] Joint School of National University of Singapore and Tianjin University, International Campus of Tianjin University, Binhai New City, Fuzhou 350207, P. R. China

[b] Department of Chemical and Biomolecular Engineering, National University of Singapore, 117585 Singapore

*Corresponding author: ning.yan@nus.edu.sg

Materials and methods

Photochemical Impedance Spectroscopy (PEIS)

Electrochemical Impedance Spectroscopy (EIS) is a useful and easy-to-use technique to evaluate the behaviour photocatalytic systems and phenomena occurring at the semiconductor/electrolyte interface, such as charge transport resistances and electron-hole recombination rates.[1] The principle of EIS is the application of by applying a small sinusoidal perturbation to the system while the amplitude and phase shift of the resulting current response are simultaneously recorded.[2, 3] To calculate capacitance of the system, the fitted model parameters for constant phase elements in the proposed ECMs are converted into equivalent capacitance by applying **Eq. (S1)**, which is related to interfacial modelling of electrochemical systems.[4, 5]

$$C_i = Q_{0,i}(\omega_{max})^{n-1} \quad \textbf{(S1)}$$

where C_i is the capacitance of circuit element i, $Q_{0,i}$ is the admittance of constant phase element i, ω_{max} is the angular frequency at which the maximum in the imaginary component of the measured impedance occurs and exponent n defines the extent of ideal capacitive behaviour: $n = 0$ for a perfect resistor while $n = 1$ for a perfect capacitor.

Fitting of PEIS data

In this work, the proposed ECMs were presented in **Fig. S1**. EIS measurements under dark condition can be modelled as a conventional Randle's circuit as shown in **Fig. S1a**. The main difference between both models would be the replacement of capacitor to a constant phase element (CPE_{CT}) to model the non-ideal capacitance in the double-layer at the photoelectrode/electrolyte interface due to inhomogeneous surface of the semiconductor electrode. Resistors are included in the ECM, where R_{CT} describes the Faradaic charge transfer across the interfacial layers while R_S represents series resistance to charge transfer, including resistance related ionic conductivity of the electrolyte, resistance of FTO glass and external

contact resistance.[2] On the other hand, EIS data under both static and periodic illuminations can be fitted with ECM presented in **Fig. S1b**. In this model, there is an additional series combination of resistor and constant phase element, which is in parallel to the R||CPE circuit. The additional elements are denoted as R_{SS} and CPE_{SS} to represent the trapping of charge carriers by surface states, such as defect states (including vacancies, lattice imperfections and interstitial impurities) within the catalyst[2, 6-8] or the catalyst surface forming complexation with adsorbates.[7, 9, 10] These surface trap states generally becomes sites for surface-related non-radiative recombination by reacting with electron acceptors or donors to form radicals. As a result, presence of surface states may hinder recombination rates, thus increasing the carriers' lifetimes up to approximately microsecond time scale.[11] The quality of fit for PEIS data under periodic illumination at different duty cycles can be found in **Fig. S2**.

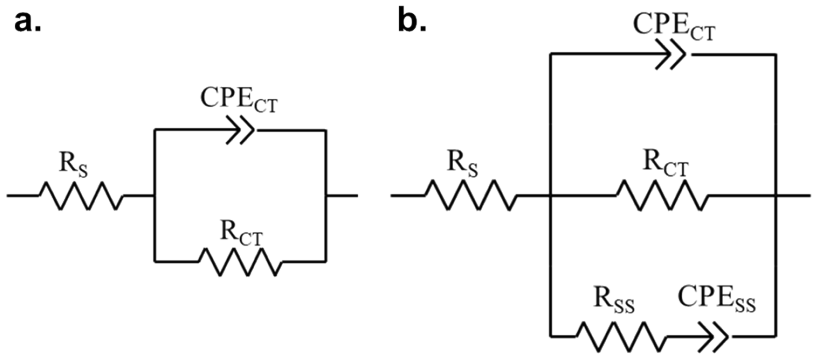

Fig. S1. Proposed ECM model for EIS measurements under **a.** dark and **b.** illumination conditions.

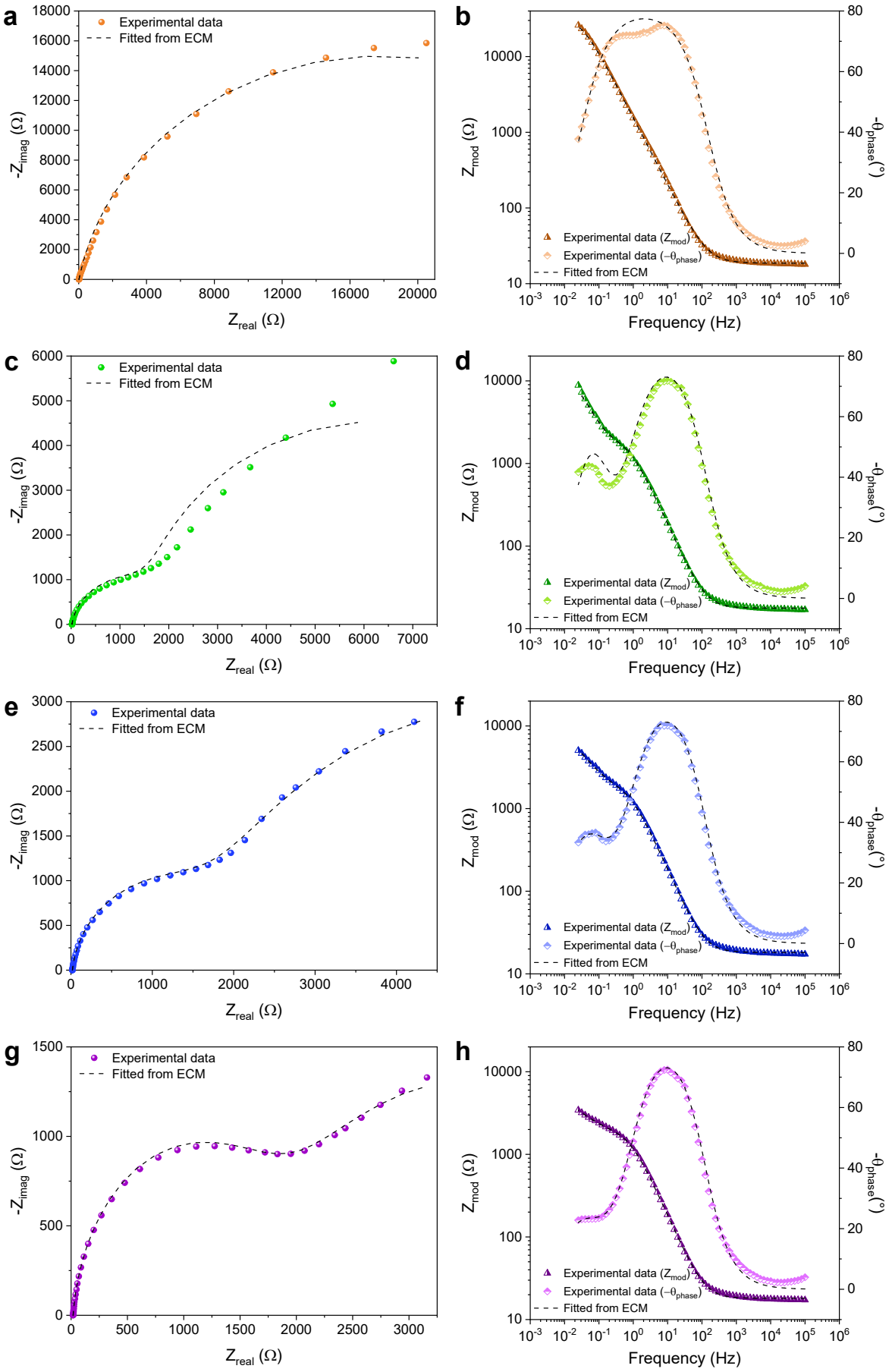
a
Experimental data
Fitted from ECM
-Z_imag (Ω)
Z_real (Ω)
b
Experimental data (Z_mod)
Experimental data (−θ_phase)
Fitted from ECM
Z_mod (Ω)
-θ_phase (°)
Frequency (Hz)
c
Experimental data
Fitted from ECM
-Z_imag (Ω)
Z_real (Ω)
d
Experimental data (Z_mod)
Experimental data (−θ_phase)
Fitted from ECM
Z_mod (Ω)
-θ_phase (°)
Frequency (Hz)
e
Experimental data
Fitted from ECM
-Z_imag (Ω)
Z_real (Ω)
f
Experimental data (Z_mod)
Experimental data (−θ_phase)
Fitted from ECM
Z_mod (Ω)
-θ_phase (°)
Frequency (Hz)
g
Experimental data
Fitted from ECM
-Z_imag (Ω)
Z_real (Ω)
h
Experimental data (Z_mod)
Experimental data (−θ_phase)
Fitted from ECM
Z_mod (Ω)
-θ_phase (°)
Frequency (Hz)

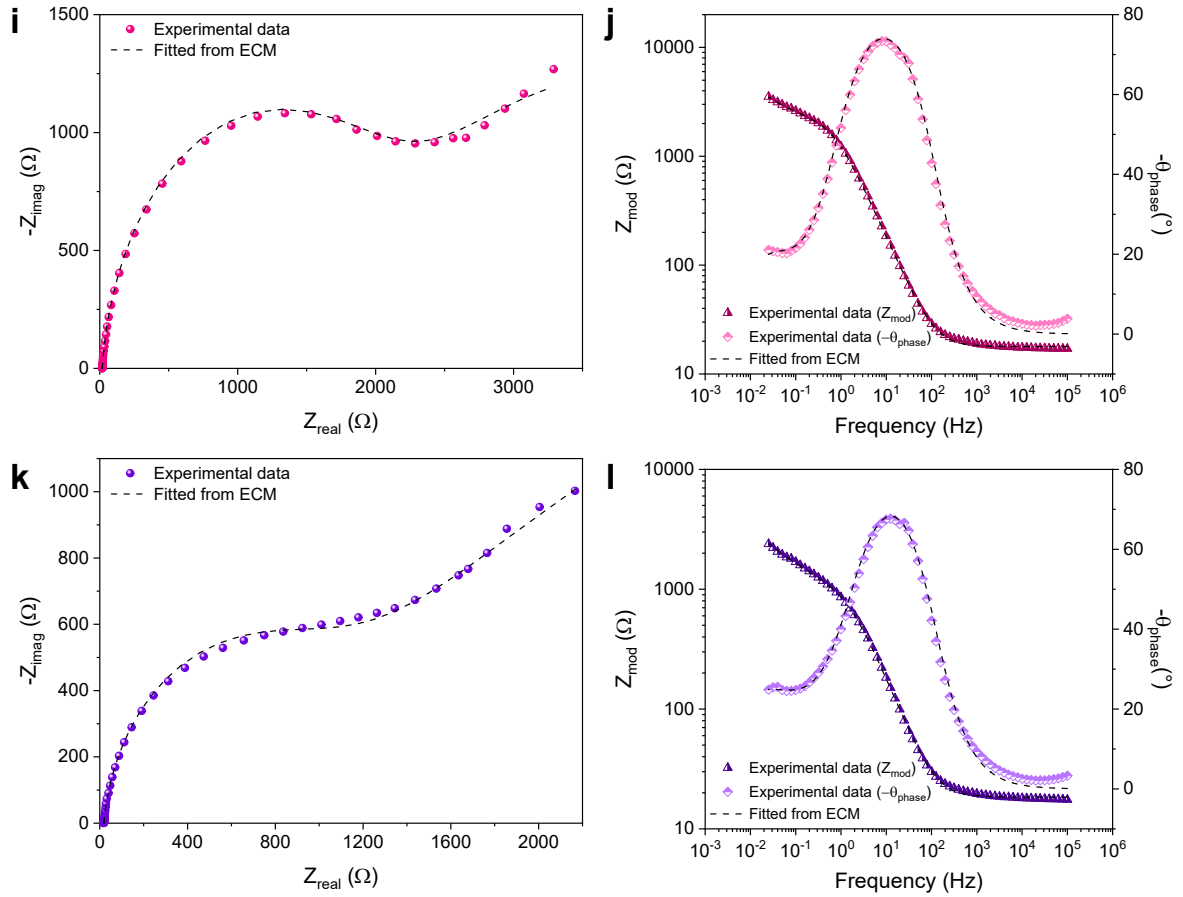

Fig. S2. Fitting of EIS data with the proposed ECM: Nyquist plot and Bode plot under (**a**, **b**) dark, periodic illumination with (**c**, **d**) 10%, (**e**, **f**) 25% and (**g**, **h**) 50%, (**i**, **j**) 75% duty cycles and (**k**, **l**) static illumination conditions respectively. Conditions: Room temperature with magnetic stirring, 50 mM HCOOH, 150 mL electrolyte solution, 25 mL/min N_2, distance between the light source and working electrode was maintained at 33 cm throughout the experiment, 3 mg Pt/TiO_2 deposited on FTO glass working electrode, Pt plate counter electrode and standard calomel reference electrode.

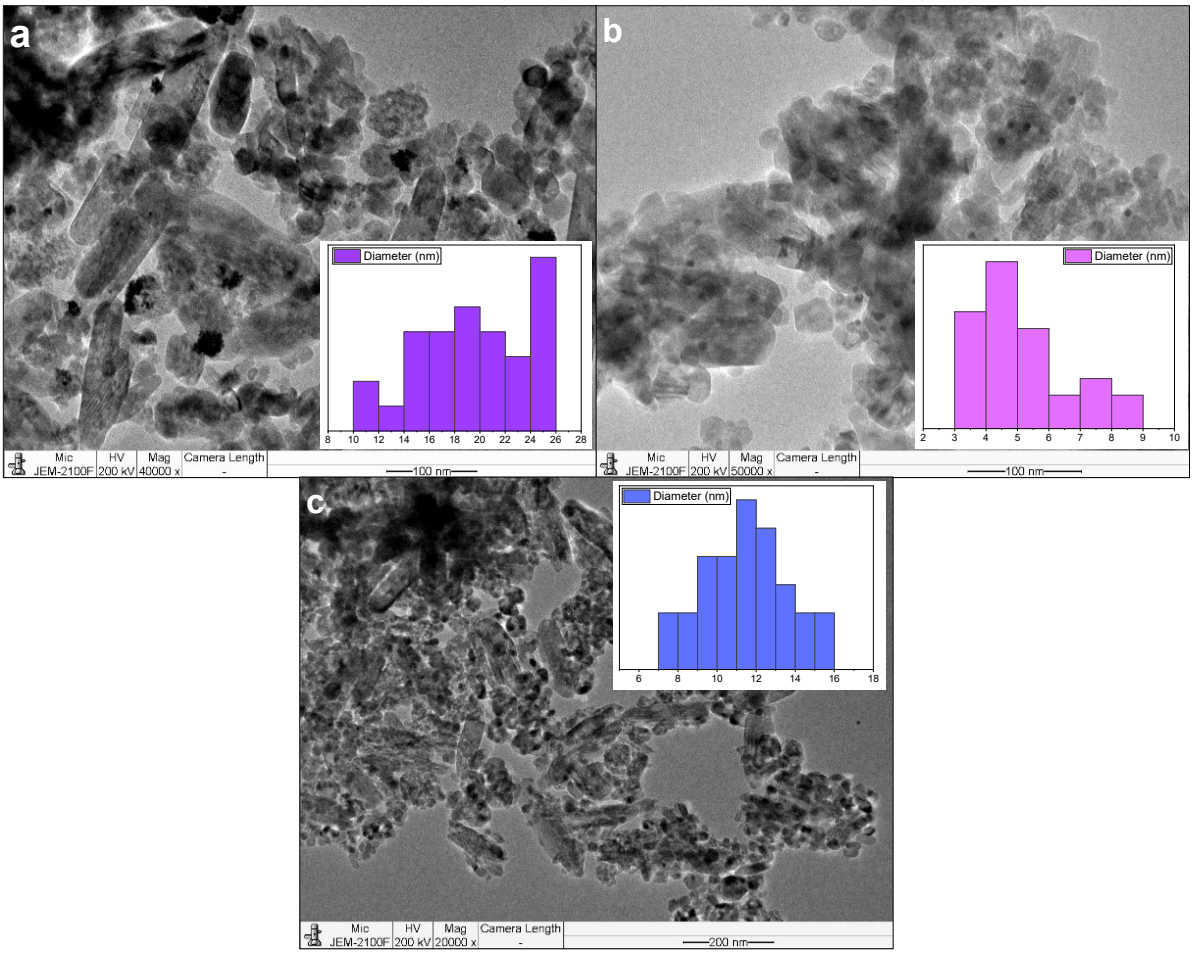

Fig. S3. TEM images for TiO_2-supported **a.** Pt, **b.** Au and **c.** Pd-supported TiO_2 catalysts.

XPS Analysis

Among the three catalysts, it is evident that their Ti 2p XPS spectra are identical with Ti $2p_{3/2}$ and $2p_{1/2}$ peaks centered at binding energies of 458.8-458.9 eV and 464.4-464.6 eV respectively as shown in **Fig. S4b**, **S4d** and **S4f**. These values are consistent with typical values of Ti^{4+} on TiO_2 via XPS analysis.[12-14] The Pt 4f spectrum is fitted with two components, where the $4f_{7/2}$ and $4f_{5/2}$ peaks located at 70.6 eV and 73.8 eV respectively are characteristic for metallic Pt^0. The other peaks with lower intensity at 73.0 eV and 76.3 eV are associated with Pt^{2+}.[15-18] Based on the relative peak areas in the Pt 4f spectrum (**Fig. S4a**), we estimate the ratio of Pt^0 to Pt^{2+} to be 2:1. Similarly, the Pd 3d XPS spectra (**Fig. S4e**) were deconvoluted into two components, where Pd^0 can be identified as $3d_{5/2}$ and $3d_{3/2}$ peaks at 335.5 eV and 340.5 eV respectively, while Pd^{2+} was identified as the corresponding peaks at 337.4 eV and 342.5 eV, likely in the form of PdO. [19-22] The Pd^0: Pd^{2+} ratio is estimated to be 7:3, similar to Pt^0: Pt^{2+} ratio in Pt/TiO_2. On the contrary, Au/TiO_2 primarily consists of metallic Au^0 nanoparticles with $4f_{7/2}$ and $4f_{5/2}$ peaks located at 83.7 eV and 87.3 eV respectively as shown in **Fig. S4c**.[12, 13]

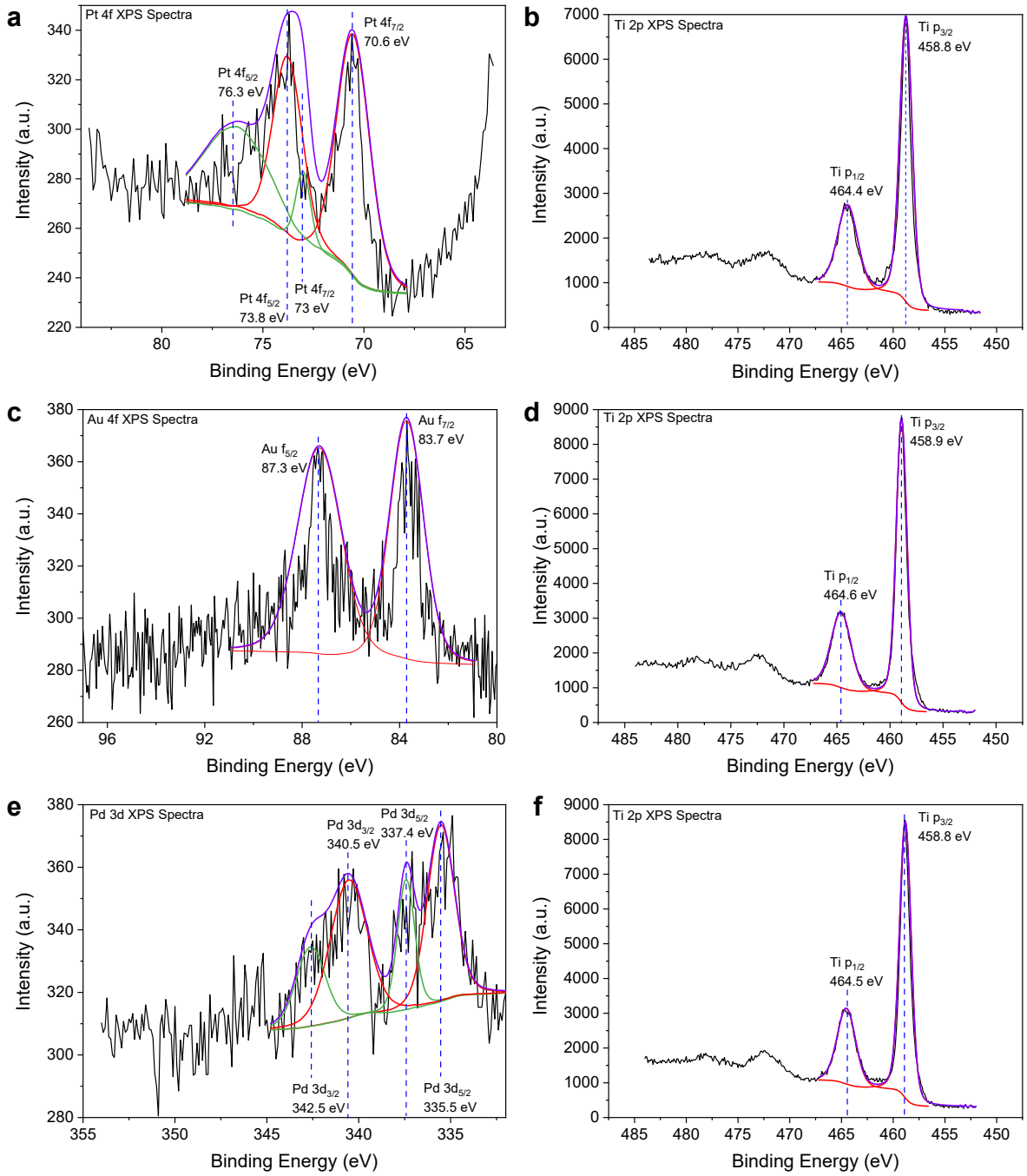

Fig. S4a. Pt 4f and **b.** Ti 2p XPS spectra of Pt/TiO_2 photocatalysts. **c.** Au 4f and **d.** Ti 2p XPS spectra of Au/TiO_2 photocatalysts. **e.** Pd 3d and **f.** Ti 2p XPS spectra of Pd/TiO_2 photocatalysts. Red line: simulated peak for element with zero valence. Green line: simulated XPS peak for element with charge of 2+. Purple line: simulated peaks for overall XPS spectrum.

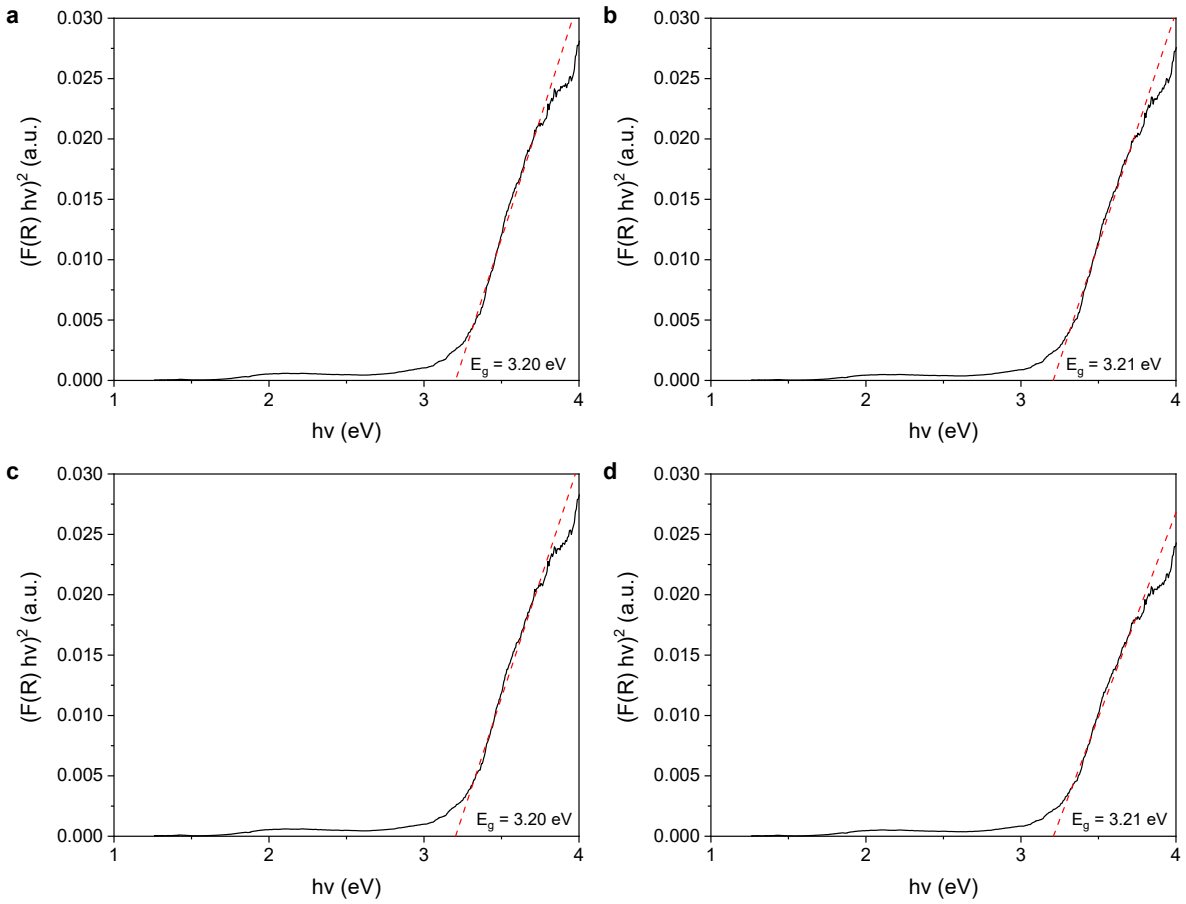

Fig. S5. Kubelka-Munk function for **a.** Bare, **b.** Pt-, **c.** Au- and **d.** Pd-supported TiO_2 catalysts.

Model fitting

The kinetic model proposed by Prozzi *et al.* is as shown below[23]:

$$\frac{k_{Deg}^{CPI}}{k_{Deg}} = (1+r)^{-1}\left\{1 + m^{-1} ln\left[1 + \frac{rm}{1+\left(\frac{\left[h_s^+\right]_2}{\left[h_s^+\right]_{ss}}\right)^{-1}}\right]\right\}$$

with

$$\frac{\left[h_s^+\right]_2}{\left[h_s^+\right]_{ss}} = \frac{rm\,tanh(m) + \sqrt{[rm\,tanh(m)]^2 + 4[rm + tanh(m)]tanh(m)}}{2[rm + tanh(m)]}$$

$$\tau_L = \sqrt{\left(k_{2,v}\bar{\emptyset}_v\right)^{-1}}$$

where k_{Deg}^{CPI} is the rate of formate degradation under controlled periodic illumination, k_{Deg} is the rate of formate degradation under static illumination, $r = \gamma^{-1}(1-\gamma)$, $m = \frac{t_{ON}}{\tau_L}$, $k_{2,v}$ is the rate constant for recombination process and $\bar{\emptyset}_v$ is the average incident photon flux introduced into the system. In this work, $k_{2,v}$ was estimated to be 3.2×10^{-11} cm^3/s and τ_L is estimated by using Bode plots (**Fig. S2**) from PEIS measurements and from Eq. (S2).

The charge carrier lifetime on Pt/TiO_2 can be estimated by Equation (S1), where f_{max} can be determined from Bode plots generated after conducting EIS analysis of Pt/TiO_2 under static and periodic illumination. f_{max} is defined as the frequency at which the maximum in the imaginary component of the measured impedance occurs.[3, 5, 9, 24, 25] According to Kern *et al.*, the medium frequency peaks (within the range of 10-100 Hz) in the Bode plot represent the properties of the photoinjected electrons within the TiO_2 and this property is independent of the TiO_2 layer thickness at f_{max}.[24]

$$\tau_e = \frac{1}{\omega_{max}} = \frac{1}{2\pi f_{max}} \quad \text{(S2)}$$

where τ_e is the lifetime of photogenerated charge carriers.

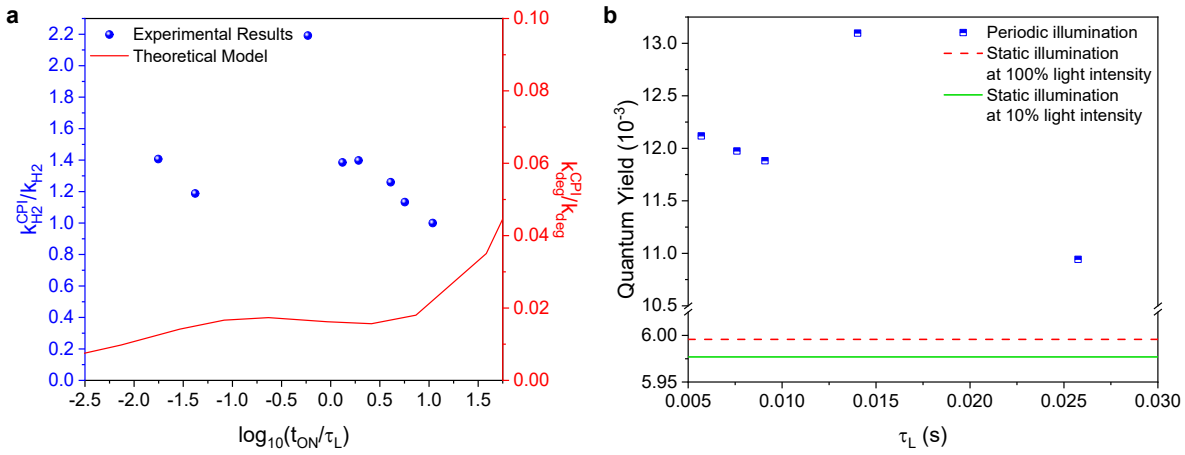

Fig. S6a. Ratio of photocatalytic reaction rate under controlled periodic illumination (CPI) and continuous illumination versus logarithm of the ratio between t_{ON} and τ_L. **b.** Comparison between reaction quantum yield under periodic illumination at 10% duty cycle and static illumination at 10% and 100% light intensity.

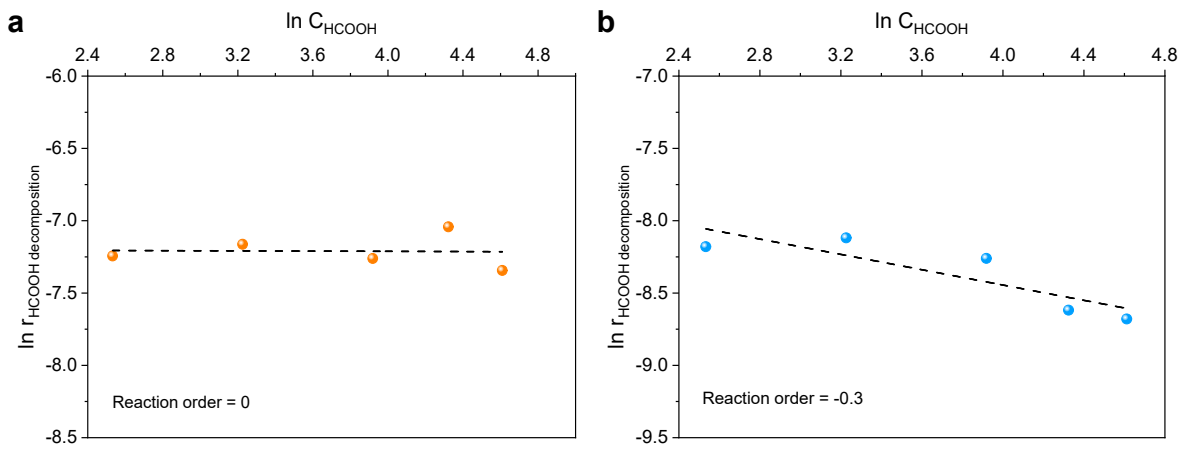

Fig. S7. Reaction kinetics of photodecomposition of HCOOH under static and periodic illumination. Plot of ln ($r_{HCOOH\ decomposition}$) against ln (C_{HCOOH}) for reaction at **a.** static illumination and **b.** periodic illumination with 10% duty cycle. Reaction conditions: 30 ± 2 °C, 30 mL reaction volume, 10 mg Pt/TiO_2, 800 rpm stirring rate, 5 bar N_2, normalised at 2 hours reaction time.

Table S1 Fitted EIS data parameters according to resistors in the proposed ECMs.

Duty Cycle (%)	R_S (Ω)		R_{CT} (Ω)		R_{SS} (Ω)	
	Average	Standard Deviation	Average	Standard Deviation	Average	Standard Deviation
0	18.40	0.35	32733	7061	-	-
10	17.65	0.10	14157	3440	2862	214
25	18.02	0.12	10811	1860	2691	132
50	17.94	0.14	6591	1403	3087	152
75	17.77	0.10	6203	351	3672	121
100	18.29	0.09	6608	1504	1339	131

Table S2 Fitted EIS data parameters according to capacitors in the proposed ECMs.

Duty Cycle (%)	C_{CT} (Ω)		C_{SS} (Ω)	
	Average	Standard Deviation	Average	Standard Deviation
0	100.27	9.48	-	-
10	85.26	1.72	317	27
25	85.48	2.25	217	28
50	86.83	1.36	283	53
75	88.48	1.93	225	32
100	85.92	2.43	156	32

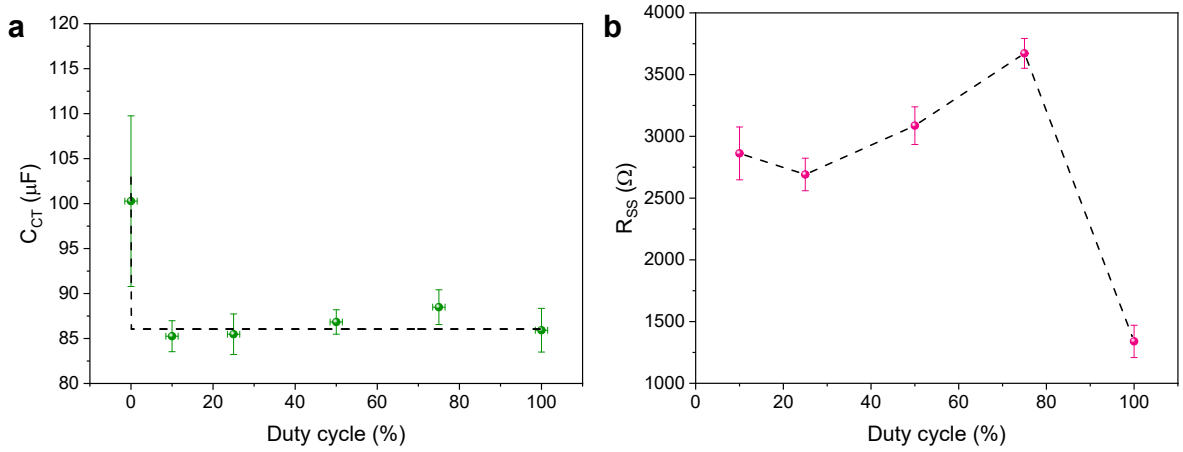

Fig. S8. a. C_{CT} and **b.** R_{SS} of Pt/TiO_2 at different duty cycles.

References

1. J. Ângelo, P. Magalhães, L. Andrade and A. Mendes, *Appl. Surf. Sci.*, 2016, **387**, 183-189.
2. A. R. C. Bredar, A. L. Chown, A. R. Burton and B. H. Farnum, *ACS Appl. Energy Mater.*, 2020, **3**, 66-98.
3. Y. Liu, D. Pan, M. Xiong, Y. Tao, X. Chen, D. Zhang, Y. Huang and G. Li, *Chinese J. Catal.*, 2020, **41**, 1554-1563.
4. A. Hankin, F. E. Bedoya-Lora, J. C. Alexander, A. Regoutz and G. H. Kelsall, *J. Mater. Chem. A*, 2019, **7**, 26162-26176.
5. S. Aslam, F. Mustafa, M. A. Ahmad, M. Saleem, M. Idrees and A. S. Bhatti, *Ceram. Int.*, 2018, **44**, 402-408.
6. J. Nelson, A. M. Eppler and I. M. Ballard, *J. Photochem. Photobiol. A*, 2002, **148**, 25-31.
7. A. J. Bard, F.-R. F. Fan, A. S. Gioda, G. Nagasubramanian and H. S. White, *Faraday Discuss. Chem. Soc.*, 1980, **70**, 19-31.
8. S. Yanagida, K. Mizumoto and C. Pac, *J. Am. Chem. Soc.*, 1986, **108**, 647-654.
9. V. Senthil, T. Badapanda, A. Chithambararaj, A. Chandra Bose and S. Panigrahi, *Int. J. Hydrog. Energy*, 2016, **41**, 22856-22865.
10. W. H. Leng, Z. Zhang, J. Q. Zhang and C. N. Cao, *J. Phys. Chem. B*, 2005, **109**, 15008-15023.
11. W. D. Kim, J.-H. Kim, S. Lee, S. Lee, J. Y. Woo, K. Lee, W.-S. Chae, S. Jeong, W. K. Bae, J. A. McGuire, J. H. Moon, M. S. Jeong and D. C. Lee, *Chem. Mater.*, 2016, **28**, 962-968.
12. H. Chen, G. Liu and L. Wang, *Sci. Rep.*, 2015, **5**, 10852.
13. N. Kruse and S. Chenakin, *Appl. Catal. A*, 2011, **391**, 367-376.
14. G. Wang, H. Wang, Y. Ling, Y. Tang, X. Yang, R. C. Fitzmorris, C. Wang, J. Z. Zhang and Y. Li, *Nano Lett.*, 2011, **11**, 3026-3033.
15. J. C. Colmenares, A. Magdziarz, M. A. Aramendia, A. Marinas, J. M. Marinas, F. J. Urbano and J. A. Navio, *Catal. Commun.*, 2011, **16**, 1-6.
16. M. Macino, A. J. Barnes, S. M. Althahban, R. Qu, E. K. Gibson, D. J. Morgan, S. J. Freakley, N. Dimitratos, C. J. Kiely, X. Gao, A. M. Beale, D. Bethell, Q. He, M. Sankar and G. J. Hutchings, *Nat. Catal.*, 2019, **2**, 873-881.
17. L. S. Kibis, D. A. Svintsitskiy, A. I. Stadnichenko, E. M. Slavinskaya, A. V. Romanenko, E. A. Fedorova, O. A. Stonkus, V. A. Svetlichnyi, E. D. Fakhrutdinova, M. Vorokhta, B. Šmíd, D. E. Doronkin, V. Marchuk, J.-D. Grunwaldt and A. I. Boronin, *Catal. Sci. Technol.*, 2021, **11**, 250-263.
18. A. Stadnichenko, D. Svintsitskiy, L. Kibis, E. Fedorova, O. Stonkus, E. Slavinskaya, I. Lapin, E. Fakhrutdinova, V. Svetlichnyi, A. Romanenko, D. Doronkin, V. Marchuk, J.-D. Grunwaldt and A. Boronin, *Appl. Sci.*, 2020, **10**, 4699.
19. F. Niu, S. Li, Y. Zong and Q. Yao, *J. Phys. Chem. C*, 2014, **118**, 19165-19171.
20. P. Wu, Y. Huang, L. Kang, M. Wu and Y. Wang, *Sci. Rep.*, 2015, **5**, 14173.
21. J. B. Zhong, Y. Lu, W. D. Jiang, Q. M. Meng, X. Y. He, J. Z. Li and Y. Q. Chen, *J. Hazard. Mater.*, 2009, **168**, 1632-1635.
22. F. Yang, Y. Xia, B. Zhang, C. Xu, W. Yang and Y. Li, *Colloids Surf. A Physicochem. Eng. Asp.*, 2021, **611**, 125785.
23. M. Prozzi, F. Sordello, S. Barletta, M. Zangirolami, F. Pellegrino, A. Bianco Prevot and V. Maurino, *ACS Catal.*, 2020, **10**, 9612-9623.
24. R. Kern, R. Sastrawan, J. Ferber, R. Stangl and J. Luther, *Electrochim. Acta*, 2002, **47**, 4213-4225.
25. M. Chandra and D. Pradhan, *ChemSusChem*, 2020, **13**, 3005-3016.